Journal of Organometallic Chemistry 695 (2010) 2586–2595

Contents lists available at ScienceDirect

Journal of Organometallic Chemistry

journal homepage: www.elsevier.com/locate/jorganchem

DFT study of substitution effect on the geometry, IR spectra, spin state and energetic stability of the ferrocenes and their pentaphospholyl analogues

Tatyana P. Gryaznova, Sergey A. Katsyuba*, Vasiliy A. Milyukov, Oleg G. Sinyashin

A.E. Arbuzov Institute of Organic and Physical Chemistry, Kazan Scientific Centre of the Russian Academy of Sciences, Arbuzov Str. 8, 420088 Kazan, Russia

ARTICLE INFO

Article history:
Received 2 March 2010
Received in revised form
1 July 2010
Accepted 20 August 2010
Available online 23 September 2010

Keywords:
Ferrocene
Pentaphosphaferrocene
DFT
IR
Spin state
Energetics

ABSTRACT

Optimal structures, vibrational spectra and thermochemical characteristics of ferrocenes and pentaphosphaferrocenes containing up to five methyl substituents in the cyclopentadienyl ring are found with the use of DFT computations. It is shown that the non-substituted ferrocenes and pentaphosphaferrocenes as well as the species with small number of methyl substituents adopt eclipsed conformations. Increasing the number of the methyl substituents results either in the conformational equilibria between the eclipsed and staggered forms or in complete shift to the staggered conformations. These effects, as well as elongation of CC bonds of the Cp ring and growth of Fe–Cp and Cp–P_5 distances with growing number of methyl groups can be explained by repulsive interactions of the methyl groups with each other or with phosphorus atoms of the pentaphospholyl ligands. The pentaphosphaferrocenes are predicted to be stable towards disproportionation to homoleptic sandwich complexes. This stability grows as the number of methyl substituents in cyclopentadienyl ring increases, which is a result of stronger Fe–P_5 bonding in the methyl substituted pentaphosphaferrocenes relative to the non-substituted species, and destabilization of the homoleptic ferrocenes because of Me···Me repulsion. A huge energy gap between the low- and high-spin states of the ferrocenes and pentaphosphoferrocenes is predicted, though introduction of methyl substituents causes a moderate decrease of the gap. Transition from low- to high-spin state should result in pronounced changes of geometry and IR spectra of the ferrocenes, which suggests that IR spectroscopy can be used for diagnostics of spin state of iron complexes.

1. Introduction

There are a great number of transition metal complexes with cyclic ligands C_nH_n. One of the most important classes is those with n = 5 (metallocenes, sandwich and half-sandwich complexes). The first synthesized such compound was ferrocene $FeCp_2$ [1], its structure being suggested by Wilkinson et al. [2]. The interest in ferrocene is related with wide application of ferrocene derivatives in catalysis, molecular electronics, polymer chemistry, nonlinear optical, magnetic and bioorganometallic materials [3]. Most of the derivatives were prepared by introducing functional groups into the cyclopentadienyl rings of ferrocene in order to tune their properties. Thus the substituted ferrocene can provide a prototype model for further understanding the properties of ferrocene-containing materials. In the last few years ferrocenes in which one or more CH groups of the Cp ligand are substituted by valence-isoelectronic group-15 elements N, P and others are widely investigated [4,5]. One of such interesting systems is pentaphosphaferrocene. Although experimental studies illustrate the potential of P_5 rings as a ligand and can lead to a wealth of interesting complexes [6], there is still not much known about the structure and bonding in complexes containing P_5 ring. For example, there are known pentaphosphaferrocenes that have from two to five alkyl substituents in cyclopentadienyl ring [7–12], but synthesis of species with fewer number of the substituents have yet failed that could be explained by influence of the substituents on stability of the pentaphosphaferrocenes. Theoretical calculations can help providing structure–property relationships. Recent studies show that density functional theory (DFT) [13] calculations are remarkably successful in predicting a variety of properties to an accuracy which rivals that of more expensive correlated *ab initio* methods. Several recent works reveal that the DFT method provides reliable results in the case of transition metal and lanthanide complexes [14]. DFT methods have been used earlier for estimation of influence of different factors on geometries, energetics and bonding in metallocenes. Frunzke et al. [4] have shown that the strength of bonding between ligand and metal atom in the ferrocene analogues $[Fe(\eta^5\text{-}E_5)_2]$ (E = N, P, As, Sb) depends on pnictogens type. Malar

* Corresponding author. Tel.: +7 8432 7318 92; fax: +7 8432 7322 53.
E-mail addresses: gryaznovat@iopc.ru (T.P. Gryaznova), skatsyuba@yahoo.com, skatsyuba@iopc.ru (S.A. Katsyuba), miluykov@iopc.ru (V.A. Milyukov).

0022-328X/$ – see front matter © 2010 Elsevier B.V. All rights reserved.
doi:10.1016/j.jorganchem.2010.08.031

[15] carried out calculations on geometries and energetics of metallocenes of Fe, Os, Ru and their phospholyl analogues and showed that P_5 ligand moves electron density on the metal center. Several works [16] devoted to the estimation of the substitution effects from different type of substituents on the geometries, the Fe–ligand interaction and the molecular electrostatic potential of ferrocene. The present study is aimed at systematically studying of the substitution effects from different number of methyl substituents on the molecular structures, vibrational spectra, stabilities and spin states of the ferrocenes and pentaphosphaferrocenes according to the hybrid DFT calculations.

2. Computational aspects

All computations reported in this study were carried out using the Gaussian 03 [17] suite of programs. Calculations were performed with Becke's three parameter hybrid exchange functional [18] and the gradient-corrected nonlocal correlation functional of Lee et al. [19] (B3LYP); Becke's exchange functional [18] in combination with Perdew and Wang 1991 gradient-corrected correlation functional [20] (BPW91); OPBE density functional, which is Handy and Cohen's optimized exchange functional OPTX [21] in combination with Perdew–Burke–Ernzerhof (PBE) functional [22].

The following basis sets were employed: a) standard 6-31G* and 6-311+G* [23]; b) "correlation consistent" cc-pVTZ basis set [24] and c) double-zeta ECP basis set of Hay and Wadt (LanL2DZ) [25]. Four different types of calculations with combined basis sets were performed: Type-I (the ligand atoms H, C, and P were treated with 6–31G* level, while for Fe atoms ECP LanL2DZ basis set was used); Type-II (the ligand atoms were treated with "correlation consistent" cc-pVTZ basis set, and 6-311+G* basis set was used for the Fe atoms), Type-III (the ligand atoms were treated with "correlation consistent" cc-pVTZ basis set, and for Fe atoms ECP LanL2DZ basis set was used) and Type-IV (the ligand atoms were treated with cc-pVTZ basis set, for the Fe atoms the 6-31G* basis set was used). Complete structural optimization was carried out for the eclipsed sandwich and the staggered sandwich geometries of the ferrocenes. All stationary points were characterized as minima by analysis of the Hessian matrices. The calculated force fields were transformed to internal coordinates, and scaling procedure was applied using the program described in Ref. [26]. The transferable scaling factors employed in this work are summarized in Supporting information, Table 1S. The scaling factor of 1.25 was taken for FeC stretchings as this value resulted in the best agreement between the calculated and the corresponding experimental vibrational frequencies. The total energies for all the optimized geometries were corrected for zero-point vibrational energy (ZPE) evaluated without scaling. For simulation of solvent effects the polarised continuum model (PCM) [27] was used.

3. Results and discussion

3.1. Geometries of ferrocene and their cyclo-P_5 analogues

The structure of ferrocene has been extensively studied from an experimental and a theoretical point of view. Experiments revealed a staggered ferrocene structure of D_{5d} symmetry in the condensed phase [28] and an eclipsed structure of D_{5h} symmetry in the gas phase [29], eclipsed conformation was also observed at 90 K in the solid [30]. Various theoretical works were performed on the ferrocene and comparison of results obtained by different methods revealed that the less costly DFT can successfully provide a good agreement between the theory and the experiment for ferrocene [14f]. So we used DFT methods to study the substituted ferrocene.

We carried out optimization of different conformations of the ferrocenes and the pentaphosphaferrocenes with 0–5 methyl substituents at B3LYP/Type-I level of theory. Some of them transformed into another during the optimization, or had imaginary frequencies after optimization. Optimal structures corresponding to minima of the potential energy surfaces of all the ferrocenes studied are shown in Fig. 1 together with their relative energies. For ferrocene **1**, pentaphosphaferrocene **7**, decaphosphaferrocene **13**, and the species **8** and **2** containing one methyl substituent on the Cp ring, only eclipsed structures were found to be stable, while the staggered sandwich conformations corresponded to transition states. Both the eclipsed and the staggered conformers were optimized for the ferrocenes **3**–**5** with two to four methyl substituents of the Cp ring and for pentaphosphaferrocenes **9**, **10** with two and three methyl groups. For pentaphosphaferrocenes **11** and **12** with four and five methyl groups and decamethylferrocene **6** we have found only staggered conformers in full agreement with crystal structure analysis [31] and electron-diffraction studies [32,33] for these compounds.

Thus the increasing number of methyl substituents in the cyclopentadienyl rings results in the shift of the eclipsed conformation of both the ferrocenes and the pentaphosphaferrocenes to the staggered forms. This conformational trend can be understood by considering the increased inter-ring repulsions when methyl groups are introduced in the cyclopentadienyl rings. The rings in ferrocene with methyl substituents are, most probably, forced into the staggered conformation by the inter-ring Me···Me repulsions: the shortest inter-ring Me···Me contacts are predicted to be 3.56 Å, somewhat shorter than twice the van der Waals radius for the methyl group (*ca.* 4 Å). In phosphaferrocenes the shortest inter-ring P···Me contacts are predicted to be 3.54 Å in the eclipsed conformation; on going to a staggered conformation it increases to 3.81 Å, while the sum of van der Waals radiuses of P and methyl group is 3.90 Å.

Selected geometrical parameters of the optimized sandwich structures are compared with available experimental values in Table 1. As a whole our computations agree satisfactorily with the available experimental [9,29–33] and the reported DFT studies [4,5,14f,15]. Structural parameters are nearly identical in both the eclipsed sandwich and the staggered sandwich arrangements. Aromatic CH bonds grow from 1.082 Å in ferrocene **1** to 1.084 Å in octamethylferrocene **5**. The corresponding force constants decrease from 5.32 to 5.23 mdyn $Å^{-1}$, which results in lower frequencies of stretching vibrations of aromatic CH bonds in the methyl-substituted ferrocenes relative to the ferrocene **1**. These and other spectroscopic effects are discussed in subsection 3.2. In the methyl groups the CH bonds directed towards Fe atom are predicted to be 0.004 Å shorter than the CH bonds directed away from Fe, both in the ferrocenes and the pentaphosphaferrocenes.

The computed C–C bond lengths in the Cp ring of the ferrocenes and pentaphosphaferrocenes are in the range 1.43–1.44 Å that agrees with the available experimental [9,29–33] and the reported DFT studies [4,5,14f,15]. Cp rings expand along the series of ferrocenes with growing number of methyl groups: the (H)C–C(H) bonds are the shortest (1.424–1.428 Å), (H)C–C(Me) bonds are a little longer (1.427–1.432 Å), and (Me)C–C(Me) bonds are the longest (1.434–1.438 Å). The lengths of the Fe–C bonds depend on the substitution in a similar way: the bonds are shorter in case of Fe–C(H) bond (2.068–2.094 Å) and longer in case Fe–C(Me) bond (2.084–2.123 Å). P–P bond lengths are quite similar for all the pentaphosphaferrocenes studied and are in the range of 2.142–2.148 Å, that is *ca.* 0.01 Å shorter than predicted by Frunzke et al. (2.153–2.158 Å) [4] and *ca.* 0.02 Å longer than the experimental values for **12** [33]. These data fully agree with Malar's [15] results.

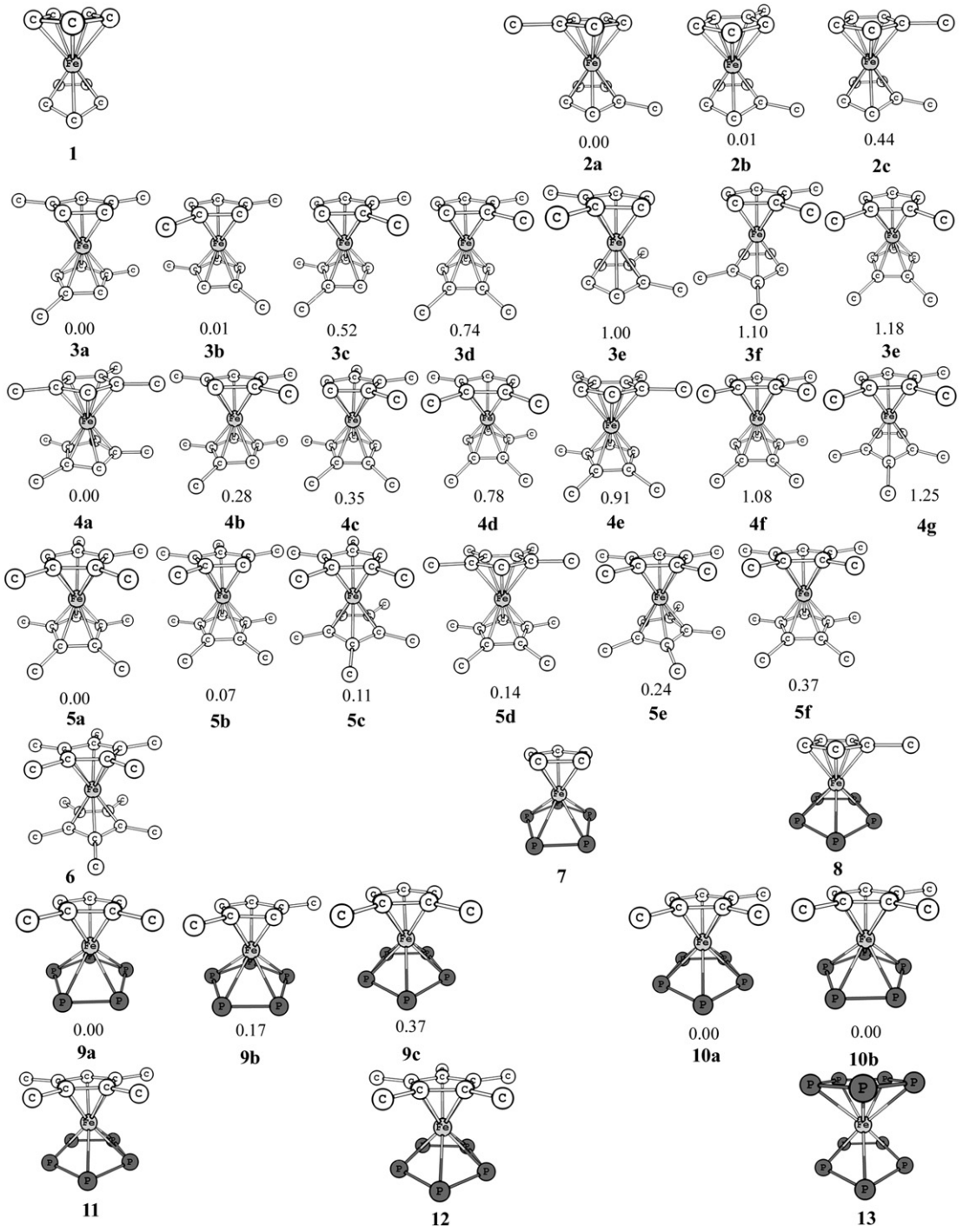

Fig. 1. Structures of ferrocenes and phosphaferrocenes, optimized at B3LYP/Type-I level of theory, and their relative energies (kcal mol^{-1}). Hydrogen atoms are omitted for clarity.

The distances between the iron atom and the center of the Cp ring in the ferrocenes **1**–**6** are predicted to be 1.687–1.696 Å. In the pentaphosphaferrocenes **7**–**12** this distance becomes longer with increasing number of methyl groups: from 1.706 Å for **7** to 1.722 Å for **12**. It seems reasonable to assume this elongation to be due to van der Waals interaction between the methyl groups and the phosphorus atoms. Smaller differences in the FeCp distances in the series of the substituted homoleptic ferrocenes **1**–**6** may be caused by higher mobility of Cp ring comparing with P_5 ligand: planes of Cp rings with introduced methyl substituents slightly deviate from each other (1–2°) to elongate Me–Me distances, while P_5 ring is fixed more rigidly. It should be mentioned that distances between the iron atom and P_5 center in the pentaphosphaferrocenes shorten from 1.623 Å for **7** to 1.619 Å for **12**, but the distance between P_5 and Cp rings grows a little in this series. In decaphosphaferrocene the distance of 1.695 Å between the iron atom and P_5 is predicted to be longer than in the heteroleptic sandwich complexes **7**–**12**, which agrees well with DFT Malar's [15] results. The lengths of Fe–P bonds in the pentaphosphaferrocenes are in the range of 2.437–2.440 Å, while in decaphosphaferrocene this value is 2.488 Å.

Table 1
Calculated bond lengths (Å) of ferrocenes and phosphaferrocenes at B3LYP/Type-I.

		Computations	Exp.
1	(H)CC(H)	1.428	1.440[a]
	FeC(H)	2.079–2.080	2.064[a]
	FeCp	1.687–1.688	1.660[a]
2a	(H)CC(H)	1.428	
	(H)CC(Me)	1.432	
	FeC(H)	2.075–2.078	
	FeC(Me)	2.089	
	FeCp	1.687	
3a	(H)CC(H)	1.428	
	(H)CC(Me)	1.430–1.431	
	FeC(H)	2.075–2.079	
	FeC(Me)	2.084–2.095	
	FeCp	1.689	
4a	(H)CC(Me)	1.430–1.432	
	(Me)CC(Me)	1.436	
	FeC(H)	2.071–2.074	
	FeC(Me)	2.081–2.093	
	FeCp	1.688	
5a	(H)CC(Me)	1.429	1.48[b]
	(Me)CC(Me)	1.436–1.438	
	CMe	1.502	1.55[b]
	FeC(H)	2.068	
	FeC(Me)	2.081–2.095	2.08[b]
	FeCp	1.691	
6	(Me)CC(Me)	1.435	1.439[c]
	CMe	1.503	1.503[c]
	FeC(Me)	2.089–2.091	2.064[c]
	FeCp	1.696	
7	(H)CC(H)	1.427	
	P–P	2.148	
	FeC(H)	2.094	
	FeP	2.444	
	FeCp	1.706	
	FeP_5	1.623	
8	(H)CC(H)	1.426	
	(H)CC(Me)	1.431	
	P–P	2.146–2.147	
	FeC(H)	2.087–2.093	
	FeC(Me)	2.120	
	FeP	2.443–2.444	
	FeCp	1.708	
	FeP_5	1.623	
9a	(H)CC(H)	1.426	
	(H)CC(Me)	1.430	
	P–P	2.146–2.147	
	FeC(H)	2.087–2.094	
	FeC(Me)	2.115	
	FeP	2.441–2.443	
	FeCp	1.712	
	FeP_5	1.621	
10a	(H)CC(H)	1.424	
	(H)CC(Me)	1.429	1.407–1.430[d]
	(Me)CC(Me)	1.437	1.457–1.470[d]
	P–P	2.145–2.147	2.069–2.105[d]
	FeC(H)	2.081	2.071–2.081[d]
	FeC(Me)	2.116–2.123	2.116–2.135[d]
	FeP	2.439–2.443	2.370–2.411[d]
	FeCp	1.715	1.717–1.727[d]
	FeP_5	1.620	1.549–1.617[d]
11	(H)CC(Me)	1.427	
	(Me)CC(Me)	1.435–1.438	
	P–P	2.145–2.146	
	FeC(H)	2.082	
	FeC(Me)	2.110–2.115	
	FeP	2.437–2.441	
	FeCp	1.718	
	FeP_5	1.618	
12	(Me)CC(Me)	1.434–1.435	1.438[e]
	P–P	2.144–2.145	2.117[e]
	FeC(Me)	2.110–2.111	2.135[e]
	FeP	2.439–2.440	2.377[e]
	FeCp	1.722	1.750[e]
	FeP_5	1.619	1.551[e]
13	P–P	2.142	
	FeP	2.488	
	FeP_5	1.695	

[a] Ref. [29b].
[b] Ref. [31a].
[c] Ref. [32].
[d] From X-ray for (η^5-1,2,4-tri-t-butylcyclopentadienyl)-(η^5-pentaphosphacyclopentadienyl)-iron Ref. [9].
[e] Ref. [33].

Different experimental and theoretical observations [9,14f,31–33] in ferrocenes and phosphaferrocenes reveal that while the aromatic CH bonds are bent out of the plane of the Cp ring towards the metal atom, the C–Me bonds are bent out of the plane away from Fe. The present study predicts the right direction of this bending of the CH and C–Me groups in the ferrocenes and pentaphosphaferrocenes. This trend again may be explained by assumption about Me···Me and P···Me repulsive interaction.

3.2. IR spectra

The present calculations of IR spectra are compared in Table 2 with experimental data, available for ferrocene **1** [34], dimethylferrocene **2** [35] and decamethylferrocene **6** [36,37]. In case of the dimethylferrocene optimization yields three possible eclipsed structures **2a**, **2b** and **2c** (Fig. 1) with energy differences of less than 1 kcal mol^{-1}. Only the computations for the form **2a** are considered in Table 2, as the calculated spectra for all three conformers practically coincide with each other. According to our computations, the symmetry of ferrocene **1** in a low-spin state ($S = 0$) is rather close, though *not exactly*, to D_{5h} point group, while the symmetry of molecule **1** in a high-spin state ($S = 2$) deviates from D_{5d} point group. As a result of these slight symmetry deviations from D_{5h} or D_{5d}, a degeneracy of some of the vibrational frequencies is lifted in the theoretical spectra of **1**. Nevertheless, to alleviate a comparison of the present spectra interpretation with the generally accepted assignment of the Cp ring vibrations, based on precedent literature [38], we neglect small differences (about 2–5 cm^{-1}) of such frequencies and put in Table 2 arithmetic means of their computed values. With the same purpose in view, the frequency numbering in the seventh column of Table 2 is given in accord with D_{5h} symmetry for low-spin ferrocene **1**.

In a whole quantum-chemically predicted vibrational frequencies agree well with the experiment, and theoretical interpretation of the spectra is very close to the empirical bands assignment published earlier [34–37]. For brevity purposes we shall not discuss typical group bands associated with stretching vibrations of the methyl groups (νCH_3), and focus on quantum-chemical description of the spectral differences caused by changes of vibrations of the aromatic fragments of the three molecules.

Experimental stretching frequencies νCH of aromatic CH groups of dimethylferrocene **2** [35] are *ca.* 10–30 cm^{-1} lower than in the case of low-spin ferrocene **1** [34]. Quantum-chemical calculations reproduce this trend only qualitatively: the νCH bands with the highest intensities are predicted at *ca.* 3123 cm^{-1} for **1** and at *ca.* 3114 cm^{-1} for **2**, the lowering of *ca.* 9 cm^{-1} being caused by differences in the force constants of CH bonds of **2** relative to **1** as discussed above.

Essential differences are found in computed frequencies of breathing modes of Cp ring. In the low-spin ferrocene **1** this mode is predicted at *ca.* 1140 cm^{-1} while the corresponding experimental IR band is found at 1112 cm^{-1} and Raman band at 1105 cm^{-1}.

Table 2
Experimental and calculated at B3LYP/Type-I level of theory IR spectra of ferrocene, dimethylferrocene and decamethylferrocene.

Assignments[a]	decamethylferrocene **6**		dimethylferrocene **2a**		ferrocene **1**			Assignments[a]
	Experiment[b] (solid) ν/cm^{-1}, I[f]	Computations[c] ν/cm^{-1} (I/km·mole^{-1})	Experiment[d] (gas) ν/cm^{-1}, I[f]	Computations ν/cm^{-1} (I/km·mole^{-1})	Experiment[e] (gas) ν/cm^{-1}, I[f]	Computations ν, cm^{-1} (I/km·mole^{-1}), a,[g] b[h]		
						$S = 0$	$S = 2$	
			3073 s	3126 (1), 3126 (11), 3114 (21), 3113 (3), 3104 (9), 3104 (1), 3101 (0), 3100 (1)	*3099 (R)* 3106 m *3085 (R)*	3134 (0), A_1', 1 3134 (3), A_2'', 8 3123 (46), E_1', 12 3122 (0), E_1'', 18 3108 (0), E_2', 23 3107 (0), E_2'', 29	3126(0), 3126(4), 3114(26), 3113(0), 3099(0), 3097(0)	νCH
δCH_3, νCC	1478 m 1476 (R)	1499 (0), 1497 (0), 1497 (2), 1497 (3), 1484 (20), 1478 (0), 1474 (14), 1470 (0), 1464 (6), 1464 (35)	1475 m 1479 (R)	1497 (0), 1497 (1)				
	1452 m 1449 (R)	1456 (1), 1453 (1), 1450 (2), 1449 (0), 1447 (0), 1445 (0), 1445 (0), 1441 (0), 1438 (0), 1437 (0)	1458 m	1459 (7), 1458 (12)				
νCC (Cp, CCp), δCH_3		1436 (0), 1434 (0), 1434 (4), 1433 (4)	1438 vw	1446 (6), 1445 (0)				
Breathing, δCH_3	1428 m *1425 (R)*	1432 (6), 1432 (0)						
νCC (Cp, Me-Cp), δCH_3		1422 (0), 1420 (0), 1409 (0), 1407 (0), 1400 (4), 1393 (3)	1412 w (liq)	1416 (1), 1415 (0)	1416 w 1408 (R)	1441 (4), E_1', 13 1440 (0), E_1'', 19	1453 (2), 1446 (0)	Asymmetric stretch νCC: C_5H_5; in plane δCCH
Breathing in-phase	*1386 (R)*	1392 (0)						
νCC (Cp, Me-Cp), δCH_3		1390 (1)	1383 m *1388 (R)*	1401 (0), 1395 (6), 1384 (0), 1383 (2)	1356 (R)	1381 (0), E_2', 24 1361 (0), E_2'', 30	1367(0), 1358 (0)	Asymmetric stretch νCC: C_5H_5; in plane δCCH
Breathing out-of-phase	1378 s	1389 (8)						
νCC (Cp, Me-Cp), δCH_3	*1367 (R)*	1386 (0), 1377 (0), 1376 (0), 1375 (0), 1374 (0)	1370 m 1371 (R)	1361 (0)				
			1341 w 1347 (R)	1354 (1)				νCC, δCCC
			1260 w	1246 (0), 1245 (1)	*1257 (sd)*	1264 (0), A_2', 7 1264 (0), A_1'', 5	1266(0)	δCCH
			1228 m 1229 (R)	1242 (3), 1241 (0)				breathing, νCMe, δCCH
νCC δCCH, δCCC	*1225 (R)*	1163 (0), 1163 (0), 1151 (0), 1149 (0)						
δCCH, δCCC		1114 (0), 1114(0)			1112 s *1105 (R)*	1141 (15), A_2'', 9 1140 (0), A_1', 2	1125 (0), 1120(1)	breathing
νCC, ρCH_3	1075 m *1068 (R)*	1077 (11), 1076 (12), 1072 (0), 1072 (0)	*1115 (R)* 1105 w *1106 (R)* 1038 s *1040 (R)*	1063 (0), 1062 (3), 1054 (0), 1054(16), 1043 (12), 1042 (2)	*1050 (R)*	1059 (0), E_2', 25 1050 (0), E_2'', 31	1060(0), 1056(0)	δCCH
ρCH_3, ring-packering	*1036 (R)* 1032 ms	1050 (8), 1049 (1), 1047 (1), 1046 (39), 1045 (10), 1045 (5), 1043 (7), 1041 (15), 1039 (1), 1037 (0)						
			1024 m *1025 (R)* 1000 w *1000 (R)*	1033 (11) 1031 (1)	1012 s *1010 (R)*	1017 (34), E_1', 14 1010 (0), E_1'', 20	1018(66), 1010(0)	δCCH
ρCH_3			*973 (R)*	981 (0), 980 (0)				δCCH

νCC		953 (0), 952 (0), 951 (0), 951 (0)	922 m	929 (8), 929 (1)				δCCC
			923 (R)					
			880 (R)	881 (2), 880 (0),		889 (0), E_2', 26	874(0), 863(0),	γCH
						880 (0), E_2'', 32		
			849 (R)	851 (0), 850 (0),		853(0), E_2', 27	845(0)	δCCC
			850 w	848 (1)846 (10)	840 w	841 (10), E_1', 15	776(207)	γCH
						837 (0), E_2'', 33	840(0)	δCCC
			818 m, 794 s	831 (45), 822 (2),	816 s	826 (0), A_1', 3	789(0), 773(93),	γCH
				812 (3), 796 (12)	776 w	825 (79), A_2'', 10	752(0)	
						808 (1), E_1'', 21		
νCMe, νCC, ρCH_3	*794 (R)*	790 (0), 789 (0), 788 (0), 787 (0)						
δCCC			618 w	627 (2), 623 (0)				
			631 (R)					
Ring-packering	640[i]	624 (0), 621 (0), 611 (0), 609 (0)		602 (0), 601 (0),				
	618 (R)			588 (0), 586 (0)				
Breathing, νFeCp*	595 w	587 (2), 580 (0)				593 (0), E_2', 28	629(0), 617(0)	Ring-packering
	590 (R)					585 (0), E_2'', 34		
δCCMe	*550 (R)*	555 (0), 553 (0)						
	551[i]							
δCCC (Cp*)	542[i]	541 (0), 540 (0), 530 (0), 530 (0)						
			495 m	486 (18)	496 s	473 (48), E_1', 16		ring tilt
νFeCp*	515 mw	492 (0),	477 s	475 (8)	480 s	470 (13), A_2'', 11	383(36)	νFeCp
				459 (28)				
ring tilt	455 s	443 (1), 442 (2), 433 (11), 429 (13)	*402 (R)*	389 (0), 377 (1)	*388 (R)*	357 (0), E_1'', 22		ring tilt
	451 (R)							
δCp*FeCp*,γC-Me	375 m	377 (13), 377 (15)						
νFeCp*	*378 (R)*	372 (0)						
torsion CH_3,	*285 (R)*	304 (0), 302 (0), 301 (0), 300 (0),	*330 (R)*	317 (2), 309 (1)				
δCCMe	277[i], 270[i]	297 (0), 296 (0) 264 (7), 264 (7)						
	256[j]							
νFeCp*			*318 (R)*	303 (0)	*303 (R)*	292 (0), A_1', 4	237(0)	νFeCp
						212 (1), 204 (0)	ring tilt	
δCpFeCp,			*268 (R)*	266 (5)	170	165 (2), E_1', 17		δCpFeCp
torsion CH_3								
δCpFeCp,				190 (0)				
γC-Me								
torsion CH_3,	237[i]	230 (1), 224 (0), 218 (3), 211 (0),		173 (0), 168(0)			155 (0), 96 (0)	ring tilt
ring tilt	200[j]	208 (0), 203 (0), 182 (2), 178 (0),						
	187[i]	175 (0), 166 (1), 159 (0), 158 (0),						
	179(R)	153 (0), 153 (0), 148 (0), 142 (0),						
	174[i]	130 (0), 123 (0)						
	169 (R)							
δCpFeCp		114 (0), 104 (0)		138 (0), 110 (0)			63 (1), 57 (1),	δCpFeCp
Ring internal		12 (0)		28 (0)		41 (0), A_1'', 6	6 (0)	Ring internal
rotation								rotation

[a] ν, stretch; δ, bend; ρ, rocking; γ, out-of-plane.
[b] Ref. [36].
[c] Symmetry of molecule **6** deviates from D_{5d} point group.
[d] Ref. [35].
[e] Ref. [34].
[f] w, weak; m, medium; s, strong; (*R*).from Raman spectrum of solid sample; (sd), from IR spectrum of solid sample.
[g] Symmetry type according to D_{5h} point group for ferrocene (see text).
[h] Numbering referring to D_{5h} point group of ferrocene (see text).
[i] From IR and Raman spectra of NaCp*, Ref. [39].
[j] Ref. [37].

Calculated breathing mode of dimethylferrocene **2** at *ca.* 1240 cm^{-1} agrees with the experimental band at *ca.* 1230 cm^{-1}. This increase of frequency compared with ferrocene **1** is caused by vibrational interaction of the breathing mode with the C-Me stretching vibrations. For decamethylferrocene **6** calculations predict three breathing modes: mixed with C-Me stretching – at 1432 cm^{-1}; mixed with CH_3 bending – at *ca.* 1390 cm^{-1}, and mixed with metal–ligand stretchings – at *ca.* 580 cm^{-1}, which correspond to experimental bands at 1428 (IR)/1425 (Raman), 1386 (Raman)/1378 (IR) and 595 (IR)/590 (Raman) cm^{-1} respectively. Higher values of the first two frequencies compared to the ferrocene **1** are caused by the reasons analogous to the case of the dimethylferrocene **2**. Decrease of the latter frequency we associate mainly with bigger mass of Me groups in **6** comparing with H atoms in **1**. So, in contrast to the case of νCH frequencies, all the dramatic changes discussed in this paragraph are caused by kinematical rather than dynamical reasons.

Experimental IR spectrum of decamethylferrocene **6** contains two bands, at 515 and 455 cm^{-1}, associated with metal–ligand motion, while in the spectrum of dimethylferrocene **2** these bands lie at 477 and 495 cm^{-1}, and in the spectrum of ferrocene **1** – at 480 and 496 cm^{-1}. According to computations the band at 515 cm^{-1} in the decamethylferrocene spectrum corresponds to the bands 480 cm^{-1} and 477 cm^{-1} in the spectra of ferrocene and dimethylferrocene, respectively, and should be assigned to Fe–Cp stretchings. IR bands at 496 and 495 cm^{-1} in the spectra of ferrocene and dimethylferrocene, respectively, and the band at 455 cm^{-1} in IR spectrum of decamethylferrocene, are assigned to cyclopentadienyl ring tilt vibrations.

3.3. Spin state

Theoretically the ground state of ferrocene has been predicted in several works [40,41] to have low spin. Einaga et al. [42,43] was the only group that has reported the direct observation of high-spin ferrocene. We made an attempt to estimate the influence of substituents on the energy gap between high and low-spin states of ferrocene. Swart et al. [41,44] revealed that hybrid DFT methods like B3LYP systematically favor high-spin states and demonstrated that OPBE functional is one of the best DFT functionals for the accurately predictions of energy gap between the high- and low-spin states. So, we carried out optimization of geometries and calculations of IR spectra for high- and low-spin states of ferrocenes not only with B3LYP, but also with OPBE functional. According to our OPBE/Type-I computations ferrocene **1** in ground state has low spin, and the gap between high and low-spin states is predicted to be 40.5 kcal mol^{-1} (Table 3) that agrees with Swart's [41] OPBE/TZP calculations. With increasing the number of methyl substituents the present computations predict a decrease of the gap, while a replacement of Cp ring by its pentaphospholyl analogue leads to a very small increase of the energy gap.

Table 4 represents optimized geometries of ferrocenes **1**, **6** and **12** in high- and low-spin states, calculated at OPBE/Type-I level of theory. According to the calculations, the spin transition causes notable changes of the geometries: Fe–Cp distances elongate by about 0.3 Å, Cp rings slightly shift relative to each other and, as a result, FeC and CC distances in Cp ring cease to be equal. In the phosphaferrocene PP and FeP bonds also become unequal and Fe–P_5 distance elongates by 0.3 Å. Optimized conformation of ferrocene **1** in high-spin state transforms from eclipsed to staggered form. Similar geometry changes are predicted by B3LYP/Type-I calculations.

Table 3
Energy gap ΔE (kcal mol^{-1}) between high- ($S = 2$) and low- ($S = 0$) spin states of ferrocenes **1**, **6** and **12** computed at OPBE/Type-I level (ZPE correction included).

Compound	ΔE
1	40.5
6	35.8
12	41.0

Table 4
Bond lengths (Å) of high- and low-spin state ferrocenes **1**, **6** and **12** calculated at OPBE/Type-I level of theory.

		$S = 0$	$S = 2$
1	CC	1.429	1.415–1.430
	FeC	1.998–1.999	2.166–2.393
	FeCp	1.587	1.932–1.933
6	CC	1.441	1.430–1.445
	CMe	1.497–1.498	1.499–1.502
	FeC	2.036–2.038	2.188–2.459
	FeCp	1.627	1.978
12	CC	1.441	1.434–1.443
	CMe	1.494	1.496–1.498
	FeC	2.059–2.061	2.208–2.370
	FeCp	1.656	1.934
	PP	2.125–2.126	2.114–2.164
	FeP	2.365–2.367	2.382–2.808
	FeP_5	1.527	1.858

Both B3LYP/Type-I and OPBE/Type-I computations predict dramatic differences in vibrational spectra of high- and low-spin ferrocene (Fig. 2). The strongest band of metal–ligand vibrations at 475 cm^{-1} shifts to lower frequencies upon the increase of the ferrocene spin and the corresponding increase of the metal–ligand distance (Table 4). Ligand CH stretching vibrations become about 10 cm^{-1} lower in high-spin state, while the strongest band of out-of-plane CH vibrations shifts from 825 to 778 cm^{-1}. Besides, the calculations predict a growth of the band corresponding to in-plane CCH bending vibrations at 1019 cm^{-1} and a decrease of intensity and frequency of the band, corresponding to breathing mode of Cp ring (1141 cm^{-1} in low-spin state and 1120 cm^{-1} in high-spin state). A comparison of the calculated spectra with the experimental IR spectrum [34] (Table 3) allows to conclude that the latter corresponds to

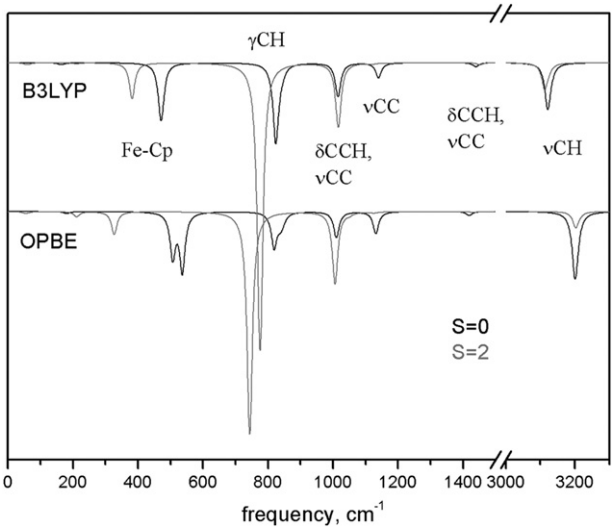

Fig. 2. Vibrational spectra of ferrocene with spin $S = 0$ and $S = 2$, calculated at B3LYP/Type-I and OPBE/Type-I level of theory. The simulated spectra are obtained by convolution of computed band intensities with a Lorentzian lineshape function (f.w.h.m. = 10 cm^{-1}).

Table 5
Energies (kcal·mol^{-1}) of reactions, calculated by different methods and standard deviations (SD) of the computations from the corresponding experimental data.

Method	$FeCp_2 \rightarrow Fe^{+2} + 2Cp^-$	$FeCp_2 \rightarrow Fe^0 + 2Cp^0$	$FeCp_2 \rightarrow Fe^0 + 5C_2H_2$	SD
BPW91/6-31G*	−702	−211	−392	81
BPW91/6-311 + G*	−665	−175	−335	29
BPW91/Type-II	−675	−177	−333	34
BPW91/Type-I	−677	−159	−338	34
B3LYP/6-31G*	−656	−154	−325	17
B3LYP/Type-II	−626	−139	−282	27
B3LYP/Type-I	**−638**	**−128**	**−299**	24
OPBE/6-31G*	−688	−214	−409	86
OPBE/Type-IV	−681	−189	−401	73
Experiment	−635 ± 15[a]	−158±2[a]	−314.5[b]	–

[a] Ref. [45].
[b] Ref. [46].

low-spin state of ferrocene, in full agreement with literature data on ground spin state of ferrocene [40–43] and with the computations of the energy gap between high- and low-spin states discussed above.

3.4. Energetics

One of the questions that will be addressed in this paper concerns the ability of heteroleptic pentaphosphaferrocenes **7**–**12** to disproportionation reaction. As it was mentioned in the introduction, while there are known pentaphosphaferrocenes that have from two to five alkyl substituents in pentadienyl ring, the species with fewer number of substituents have not yet been obtained. One of possible explanations of this fact is an assumption that pentaphosphaferrocene **7** disproportionates easily to clear homoleptic ferrocenes **1** and **13**: $2FeCpP_5(\mathbf{7}) \rightarrow Fe(Cp)_2(\mathbf{1}) + Fe(P_5)_2(\mathbf{13})$, whereas a disproportionation reaction for pentamethylpentaphosphaferrocene **12**: $2FeCp^*P_5(\mathbf{12}) \rightarrow Fe(Cp^*)_2(\mathbf{6}) + Fe(P_5)_2(\mathbf{13})$, where Cp^* is the pentamethylcyclopentadienyl, is energetically disadvantageous because of stabilization of pentaphosphaferrocene **12** by the methyl substituents.

To choose a method adequately describing relative energies of various ferrocenes, the results of several calculations with different basis sets and DFT functionals were compared with available experimental data. Table 5 shows the relative stabilities of the complexes with reference to their ionic components, their neutral components and with reference to Fe atom and ethylene. The dications of the metals were calculated at their ^5D ground state.

The best predictions of the dissociation energies for the eclipsed geometry of ferrocene are based on the B3LYP/6-31G* calculations, but the energies predicted by the B3LYP/Type-I and B3LYP/Type-II are very close to those of the all-electron 6-31G* results. So, the least computationally expensive B3LYP/Type-I computations, used in the present work for analysis of the binding energies of the substituted ferrocenes, are expected to be reliable.

The dissociation energies predicted in this work by BPW91/6-311+G* computations for ferrocene show almost the same agreement with the experimental data as the results obtained by using the B3LYP functional. It was demonstrated earlier [47] that BPW91 calculations of the thermochemical characteristics of polyphosphorus compounds were of superior quality in comparison with other DFT functionals. Similar conclusion was obtained on the basis of comparison of BPW91 results with CCSD(T) predictions for the mechanism of protonation of ferrocene [48]. So, for higher reliability of our predictions for the pentaphosphaferrocenes we computed the energy difference between homo- and heteroleptic ferrocenes by both the methods. Tables 6 and 7 represents the energies of the disproportionation reactions of the pentaphosphaferrocenes **7** and **12**, respectively, calculated using BPW91 and B3LYP functionals with different basis sets, both in vacuo and in the diethylether solvent treated as a polarisable continuum. All the methods used yield qualitatively similar results: the both phosphaferrocenes are predicted to be stable towards disproportionation reaction, though the substituted phosphaferrocene **12** is more stable than the phosphaferrocene **7**.

It is clearly seen from Tables 6 and 7 that the calculated energies of the disproportionation reactions practically do not depend on the method used. Thus, B3LYP/Type-I was chosen for further calculations as a computationally inexpensive approach, which allows achieving accuracy sufficient for the abovementioned purposes. We estimated energies of disproportionation reactions for the pentaphosphaferrocenes **7-12** (Table 8). These data demonstrate that the more methyl groups are introduced in the cyclopentadienyl ring the higher is stability of the corresponding pentaphosphaferrocene towards the disproportionation reaction.

The increase of ΔE values in the series **7**–**12** (Table 8) is caused by two factors: (i) destabilization of the homoleptic ferrocenes with introducing of methyl substituents into Cp ring because of Me···Me repulsion; (ii) stabilization of the methyl substituted pentaphosphaferrocenes compared to the non-substituted heteroleptic species. Table 9 demonstrates these trends by the example of ferrocenes **1** and **6**, and pentaphosphaferrocenes **7** and **12**. The increasing of heterolytic dissociation energy in the substituted phosphaferrocenes, in spite of Me···P repulsion, is associated with the higher strength of Fe–P_5 bonding. Indeed, the computations predict small shortening of Fe–P_5 distance (Table 1) and essential increase of frequency of stretching vibrations Fe–P_5 (from 206 cm^{-1} for **7**–250 cm^{-1} for **12**) [49].

Table 6
Energies and Gibbs free energies of disproportionation reaction of pentaphosphaferrocene **7**, calculated by different methods.

	BPW91/6-31G*	BPW91/6-311+G*	BPW91/Type-II	BPW91/Type-II in diethylether	B3LYP/Type-I	B3LYP/Type-III
ΔE, kcal mol^{-1}	27	22	20	23	18	18
ΔG, kcal mol^{-1}	25	23	21	21	17	16

Table 7
Energies and Gibbs free energies of disproportionation reaction of pentaphosphaferrocene **12**, calculated by different methods.

	BPW91/6-31G*	BPW91/Type-II in diethylether	B3LYP/Type-I
ΔE, kcal mol^{-1}	45	34	30
ΔG, kcal mol^{-1}	46	33	33

Table 8
Energy of disproportionation reactions of pentaphosphaferrocenes with 0–5 methyl substituents in Cp ring, calculated at B3LYP/Type-I level on theory.

Reaction	ΔE, kcal mol^{-1}
2× **7** → **13** + **1**	18
2× **8** → **13** + **2a**	20
2× **9a** → **13** + **3a**	22
2× **9b** → **13** + **3c**	22
2× **10a** → **13** + **4a**	24
2× **11** → **13** + **5a**	27
2× **12** → **13** + **6**	31

Table 9
Heterolytic dissociation energies of the ferrocenes and pentaphosphaferrocenes with 0 and 5 methyl substituents in Cp ring.

	Reaction[a]	ΔE, kcal mol^{-1}
1	$FeCp_2 \rightarrow Fe^{2+} + 2Cp^-$	−638
6	$FeCp^*_2 \rightarrow Fe^{2+} + 2Cp^{*-}$	−629
7	$FeP_5Cp \rightarrow Fe^{2+} + P_5^- + Cp^-$	−582
12	$FeP_5Cp^* \rightarrow Fe^{2+} + P_5^- + Cp^{*-}$	−584

[a] Cp^* – pentamethylcyclopentadienyl.

4. Conclusions

The results of this work can be summarized as follows.

It is shown that calculations with the use of B3LYP functional in combination with 6–31G* basis set for ligands' atoms and LanL2DZ for Fe atoms reproduce reliably geometry, vibrational spectra and thermochemical characteristics of ferrocenes.

We have found optimal structures for the ferrocenes and phosphaferrocenes containing up to five methyl substituents in the cyclopentadienyl ring. The non-substituted ferrocenes and phosphaferrocenes as well as the species with small number of methyl substituents adopt eclipsed conformations. Increasing the number of the methyl substituents results either in the conformational equilibria between the eclipsed and staggered forms or in complete shift to the staggered conformations. These effects can be explained by repulsive interactions of the methyl groups with each other or with phosphorus atoms of the phospholyl ligands.

The abovementioned interactions cause elongation of CC bonds of the Cp ring and growth of Fe–Cp and Cp–P_5 distances with growing number of methyl groups in the aromatic moiety, though Fe–P_5 distances become even slightly smaller in the same series.

The computations predict pentaphosphaferrocenes to be stable towards disproportionation to homoleptic sandwich complexes. The stability of the phosphaferrocenes towards the disproportionation reaction grows as the number of methyl substituents in cyclopentadienyl ring increases. This trend is explained by stronger Fe–P_5 bonding in the methyl substituted pentaphosphaferrocenes relative to the non-substituted species, and destabilization of the homoleptic ferrocenes with introducing of methyl substituents into Cp ring because of Me⋯Me repulsion.

According to our computations both ferrocenes and pentaphosphoferrocenes in ground state have low spin ($S = 0$), and the energy gap between the low- and high-spin ($S = 2$) states is predicted to exceed 40 kcal mol^{-1}, though introduction of methyl substituents causes a small decrease of the gap. Transition from low- to high-spin state results in: (i) a pronounced elongation of Fe–Cp distances, (ii) a shift of the ligand rings relative to each other and (iii) a transformation of eclipsed ferrocene conformation to staggered conformation. Calculated IR spectra of ferrocene in the low- and high-spin states have notable differences and the computed spectrum of the low-spin ferrocene agrees much better with experimental IR spectrogram, than the spectrum predicted for the high-spin ferrocene. This latter result suggests that IR spectroscopy can be used for diagnostics of spin state of transition metal complexes, which will be a subject of a separate publication.

Acknowledgments

The authors are indebted to all staff-members of the Supercomputer centre of the Kazan Scientific Centre of the Russian Academy of Sciences and especially to Dr. D. Chachkov for technical assistance in the computations and valuable advice. Special thanks are due to Dr. M.A. Tafipolsky for permission to use his version of the program, adopted from Sipachev [26].

Appendix A. Supplementary material

Supplementary data associated with this article can be found, in the online version at doi:10.1016/j.jorganchem.2010.08.031.

References

[1] (a) T.J. Kealy, P.L. Pauson, Nature 168 (1951) 1039–1040;
(b) S.A. Miller, J.A. Tebboth, J.F. Tremaine, J. Chem. Soc. (1952) 632–635.
[2] G. Wilkinson, M. Rosenblum, M.C. Whiting, R.B. Woodward, J. Am. Chem. Soc. 74 (1952) 2125–2126.
[3] (a) R. Rulkens, A.J. Lough, I. Manners, S.R. Lovelace, C. Grant, W.E. Geiger, J. Am. Chem. Soc. 118 (1996) 12683–12695;
(b) M. Refaei, L.I. Espada, M. Sharadam, in: Proceedings of SPIE, vol. 4036, The International Society for Optical Engineering, 2000, pp. 123–131;
(c) A.E.-W. Sarhan, Y. Nouchi, T. Izumi, Tetrahedron 59 (2003) 6353–6362;
(d) C. Paquet, P.W. Cyr, E. Kumacheva, I. Manners, Chem. Commun. 10 (2004) 234–235;
(e) D.R. Van Staveren, N. Metzler-Nolte, Chem. Rev. 104 (2004) 5931–5985;
(f) R.K. Nagarale, J.M. Lee, W. Shin, Electrochim. Acta 54 (2009) 6508–6514;
(g) J.-D. Qiu, M. Xiong, Biosens. Bioelectron. 24 (2009) 2649–2653.
[4] J. Frunzke, M. Lein, G. Frenking, Organometallics 21 (2002) 3351–3359.
[5] G. Frison, F. Mathey, A. Sevin, J. Phys. Chem. A 106 (2002) 5653–5659.
[6] (a) J. Bai, A.V. Virovets, M. Scheer, Science 300 (2003) 781–783;
(b) M. Scheer, A. Schindler, C. Gröger, A.V. Virovets, E.V. Peresypkina, Angew. Chem. Int. Ed. 48 (2009) 5046–5049;
(c) M. Scheer, L.J. Gregoriades, A.V. Virovets, W. Kunz, R. Neueder, I. Krossing, Angew. Chem. Int. Ed. 45 (2006) 5689–5693.
[7] O.J. Scherer, T. Bruck, Angew. Chem. 99 (1987) 59.
[8] O.J. Scherer, T. Bruck, G. Wolmershauser, Chem. Ber. 121 (1988) 935–938.
[9] O.J. Scherer, T. Hilt, G. Wolmershauser, Organometallics 17 (1998) 4110–4112.
[10] V.A. Miluykov, O.G. Sinyashin, O. Scherer, E. Hey-Hawkins, Mendeleev Commun. 12 (2002) 1–2.
[11] F. Dielmann, R. Merkle, S. Heinl, M. Scheer, Z. Naturforsch. . Sect. B. J. Chem. Sci. 64 (2009) 3–10.
[12] M. Scheer, K. Schuster, A. Krug, H. Hartung, Chem. Ber. 130 (1997) 1299–1304.
[13] (a) P. Hohenberg, W. Kohn, Phys. Rev. 136 (1964) B864–B871;
(b) R.G. Parr, W. Yang, Density Functional Theory of Atoms and Molecules. Oxford University Press, New York, 1989.
[14] (a) N. Matsuzawa, J. Seto, D.A. Dixon, J. Phys. Chem. A 101 (1997) 9391–9398;
(b) M.J. Mayor-López, J. Weber, Chem. Phys. Lett. 281 (1997) 226–232;
(c) A.M. Orendt, J.C. Facelli, Y.J. Jiang, D.M. Grant, J. Phys. Chem. A 102 (1998) 7692–7697;
(d) L. Maron, O. Eisenstein, J. Phys. Chem. A 104 (2000) 7140–7143;
(e) Z.-F. Xu, Y. Xie, W.-L. Feng, H.F. Schaefer III, J. Phys. Chem. A 107 (2003) 2716–2729;
(f) S. Coriani, A. Haaland, T. Helgaker, P. Jorgensen, ChemPhysChem 7 (2006) 245–249.
[15] E.J.P. Malar, Eur. J. Inorg. Chem. (2004) 2723–2732.
[16] (a) G. Zhang, H. Zhang, M. Sun, Y. Liu, X. Pang, X. Yu, B. Liu, Z. Li, J. Comput. Chem. 28 (2007) 2260–2274;
(b) T.-Y. Lee, P.-R. Chiang, M.-C. Tsai, C.-Y. Lin, J.-H. Huang, J. Mol. Struct. 935 (2009) 102–109.
[17] M.J. Frisch, G.W. Trucks, H.B. Schlegel, G.E. Scuseria, M.A. Robb, J.R. Cheeseman, J.A. Montgomery, T. Vreven, K.N. Kudin, J.C. Burant, J.M. Millam, S.S. Iyengar, J. Tomasi, V. Barone, B. Mennucci, M. Cossi, G. Scalmani, N. Rega, G.H. Petersson, H. Nakatsuji, M. Hada, M. Ehara, K. Toyota, R. Fukuda, J. Hasegawa, M. Ishida, T. Nakajima, Y. Honda, O. Kitao, H. Nakai, M. Klene, X. Li, J.E. Knox, H.P. Hratchian, J.B. Cross, C. Adamo, J. Jaramillo, R. Gomperts, R.E. Stratmann, O. Yazyev, A.J. Austin, R. Cammi, C. Pomelli, J.W. Ochterski, P.Y. Ayala, K. Morokuma, G.A. Voth, P. Salvador, J.J. Dannenberg, V.G. Zakrzewski, S. Dapprich, A.D. Daniels, M.C. Strain, O. Farkas, D.K. Malick, A.D. Rabuck, K. Raghavachari, J.B. Foresman, J.V. Ortiz, Q. Cui, A.G. Baboul, S. Clifford, J. Cioslowski, B.B. Stefanov, G. Liu, A. Liashenko, P. Piskorz, I. Komaromi, R.L. Martin, D.J. Fox, T. Keith, M.A. Al-Laham, C.Y. Peng, A. Nanayakkara, M. Challacombe, P.M.W. Gill, B. Johnson, W. Chen, M.W. Wong, C. Gonzalez, J.A. Pople, Gaussian 03, Revision B.05. Gaussian, Inc., Wallingford, CT, 2004.
[18] A.D. Becke, J. Chem. Phys. 98 (1993) 5648–5652.
[19] C. Lee, W. Yang, R.G. Parr, Phys. Rev. B37 (1988) 785–789.
[20] (a) J.P. Perdew, In: P. Ziesche, H. Eschrig (Eds.), Electronic Structure of Solids '91, Akademie Verlag, Berlin, 1991, p. 11;
(b) J.P. Perdew, Y. Wang, Phys. Rev. B45 (1992) 13244–13249.
[21] N.C. Handy, A.J. Cohen, Mol. Phys. 99 (2001) 403–412.
[22] (a) J.P. Perdew, K. Burke, M. Ernzerhof, Phys. Rev. Lett. 77 (1996) 3865–3868;
(b) J.P. Perdew, K. Burke, M. Ernzerhof, Phys. Rev. Lett. 78 (1997) 1396.
[23] P.C. Hariharan, J.A. Pople, Theor. Chim. Acta 28 (1973) 213–222.
[24] D.E. Woon, T.H. Dunning, J. Chem. Phys. 99 (1993) 3730–3737.
[25] (a) T.H. Dunning Jr., P.J. Hay, Modern Theoretical Chemistry, vol. 3, Plenum, New York, 1976, pp. 1–28;
(b) P.J. Hay, W.R. Wadt, J. Chem. Phys. 82 (1985) 270–283;
(c) W.R. Wadt, P.J. Hay, J. Chem. Phys. 82 (1985) 284–298;
(d) P.J. Hay, W.R. Wadt, J. Chem. Phys. 82 (1985) 299–310.

[26] (a) V.A. Sipachev, J. Mol. Struct. 567–568 (2001) 67–72;
(b) V.A. Sipachev, Struct. Chem. 11 (2000) 167–172.
[27] (a) S. Miertus, E. Scrocco, J. Tomasi, J. Phys. Chem. 55 (1981) 117–129;
(b) M. Cossi, G. Scalmani, N. Rega, V. Barone, J. Chem. Phys. 117 (2002) 43–54.
[28] (a) E.O. Fischer, W. Pfab, Z. Naturforsch. B. 7 (1952) 377–379;
(b) P.F. Eiland, R. Pepinsky, J. Am. Chem. Soc. 74 (1952) 4971;
(c) J.D. Dunitz, L.E. Orgel, Nature 171 (1953) 121–122;
(d) J.D. Dunitz, L.E. Orgel, A. Rich, Acta Crystallogr. 9 (1956) 373–375.
[29] (a) R.K. Bohn, A. Haaland, J. Organomet. Chem. 5 (1966) 470–476;
(b) A. Haaland, J.E. Nilsson, Acta Chem. Scand. 22 (1968) 2653–2670;
(c) A. Haaland, J. Lusztyk, D.P. Novak, J. Brunvoll, K.B. Starowieyski, J. Chem. Soc. Chem. Commun. (1974) 54–55.
[30] P. Seiler, J.D. Dunitz, Acta Crystallogr., Sect. B. 38 (1982) 1741–1745.
[31] (a) Yu.T. Struchkov, V.G. Andrianov, T.N. Sal'nikova, I.R. Lyatifov, R.B. Materikova, J. Organomet. Chem. 145 (1978) 213–223;
(b) D.P. Freyberg, J.L. Robbins, K.N. Raymond, J.C. Smart, J. Am. Chem. Soc. 101 (1979) 892–897.
[32] A. Almenningen, A. Haaland, S. Samdal, J. Brunvoll, J.L. Robbins, J.C. Smart, J. Organomet. Chem. 173 (1979) 293–299.
[33] R. Blom, Th Bruck, O.J. Scherer, Acta Chem. Scand. 43 (1989) 458–462.
[34] E.R. Lippincott, R.D. Nelson, Spectrochimica Acta 10 (1958) 307–329.
[35] R.T. Bailey, E.R. Lippincott, Spectrochimica Acta 21 (1965) 389–398.
[36] D.M. Duggan, D.N. Hendrickson, Inorg. Chem. 14 (1975) 955–970.
[37] L. Phillips, A.R. Lacey, M.K. Cooper, J. Chem. Soc., Dalton Trans. (1988) 1383–1391.
[38] K. Nakamoto, Infrared and Raman Spectra of Inorganic and Coordination Compounds-Part B, fifth ed. Wiley, New York, 1997, p. 286.
[39] É Bencze, B.V. Lokshin, J. Mink, W.A. Herrmann, F.E. Kühn, J. Organomet. Chem. 627 (2001) 55–66.
[40] M.L. McKee, J. Phys. Chem. 96 (1992) 1683–1690.
[41] M. Swart, Inorg. Chim. Acta 360 (2007) 179–189.
[42] Y. Einaga, Y. Yamada, T. Tominaga, J. Radioanal. Nucl. Chem. 218 (1997) 97–100.
[43] Y. Einaga, M. Kotake, Y. Yamada, O. Sato, Chem. Lett. 32 (2003) 846–847.
[44] M. Swart, A.R. Groenhof, A.W. Ehlers, K. Lammertsma, J. Phys. Chem. A 108 (2004) 5479–5483.
[45] M.F. Ryan, J.R. Eyler, D.E. Richardson, J. Am. Chem. Soc. 114 (1992) 8611–8619.
[46] S.G. Lias, J.E. Bartmess, J.F. Liebman, J.L. Holmes, R.D. Levin, W.G. Mallard, J. Phys. Chem. Ref. Data 17 (Suppl.1) (1988).
[47] S. Katsyuba, R. Schmutzler, J. Grunenberg, Dalton Trans. 9 (2005) 1701–1706.
[48] M.J. Mayor-López, H.P. Luthi, J. Chem. Phys. 113 (2000) 8009–8014.
[49] Gaussian output files for IR spectra computations can be received from the authors upon request.